Published in final edited form as:
Sci Signal. ; 7(313): ra17. doi:10.1126/scisignal.2004785.

The Adaptor Protein p66Shc Inhibits mTOR-Dependent Anabolic Metabolism

Mohamed A. Soliman[1,2,4,*], **Anas M. Abdel Rahman**[1,10], **Dudley A. Lamming**[5], **Kıvanç Birsoy**[5], **Judy Pawling**[1], **Maria E. Frigolet**[1,3], **Huogen Lu**[1,3], **I. George Fantus**[1,3], **Adrian Pasculescu**[1], **Yong Zheng**[1], **David M. Sabatini**[5,6,7,8,9], **James W. Dennis**[1,2,*], and **Tony Pawson**[1,2]

[1]Samuel Lunenfeld Research Institute, Mount Sinai Hospital, Toronto M5G 1X5, Canada

[2]Department of Molecular Genetics, University of Toronto, Toronto M5S 1A8, Canada

[3]Banting and Best Diabetes Centre, Toronto General Research Institute, Faculty of Medicine, University of Toronto, Toronto, Canada

[4]Department of Biochemistry, Faculty of Pharmacy, Cairo University, Egypt

[5]Whitehead Institute for Biomedical Research, Nine Cambridge Center, Cambridge, MA 02142, USA

[6]Department of Biology, Massachusetts Institute of Technology (MIT), Cambridge, MA 02139, USA

[7]David H. Koch Institute for Integrative Cancer Research at MIT, 77 Massachusetts Avenue, Cambridge, MA 02139, USA

[8]Broad Institute, Seven Cambridge Center, Cambridge, MA 02142, USA

[9]Howard Hughes Medical Institute, MIT, Cambridge, MA 02139, USA

Abstract

Adaptor proteins link surface receptors to intracellular signaling pathways, and potentially control the way cells respond to nutrient availability. Mice deficient in p66Shc, the most-recently evolved isoform of the Shc1 adaptor proteins and a mediator of receptor tyrosine kinase signaling display resistance to diabetes and obesity. Using quantitative mass spectrometry, we found that p66Shc inhibited glucose metabolism. Depletion of p66Shc enhanced glycolysis and increased the allocation of glucose-derived carbon into anabolic metabolism, characteristics of a metabolic shift called the Warburg effect. This change in metabolism was mediated by the mammalian target of rapamycin (mTOR), because inhibition of mTOR with rapamycin reversed the glycolytic phenotype caused by p66Shc deficiency. Thus, unlike the other isoforms of Shc1, p66Shc appears

[*]To whom correspondence should be addressed: ma.soliman@utoronto.ca (M.A.S) and dennis@lunenfeld.ca (J.W.D).
[10]Current address: School of Pharmacy, Yarmouk University, Irbid, Jordan

Dedicated to the memory of the late Dr. Tony Pawson

Competing interests: the authors declare that they have no competing interests.

Data and materials availability: The metabolomics and mass spectrometry data have been deposited at ftp://PASS00385:PU9246h@ftp.peptideatlas.org/.

to antagonize insulin and mTOR signaling, which limits glucose uptake and metabolism. Our results identify a critical inhibitory role for p66Shc in anabolic metabolism.

Introduction

A common mechanism through which activated receptor tyrosine kinases control intracellular pathways involves recruitment of SH2-containing proteins with regulatory or adaptor functions (1). For example, the Grb10 adaptor is an inhibitor of insulin signaling that is stabilized by mTOR-mediated phosphorylation and suppresses insulin sensitivity *in vivo* (2-5). Loss of inhibitors can result in dysregulation of growth factor signaling, promoting the re-wiring of metabolic pathways in a manner that supports rapid growth and cell survival. A major change that occurs in such proliferating cells is enhanced glucose uptake and catabolism, accompanied by increased lactate production, a phenomenon referred to as the "Warburg effect" (6, 7). This re-wiring provides proliferating cells with biosynthetic precursors from increased glucose-derived carbon intermediates that are essential for increasing cell biomass.

The gene for the Shc1 adaptor protein encodes three isoforms in mammals: p46, p52 and p66. These proteins share a modular arrangement of a phosphotyrosine binding (PTB) domain, a collagen homology 1 (CH1) region, and a Src homology 2 (SH2) domain (Fig. 1A). p66Shc and p52Shc or p46Shc (p52/p46Shc) are encoded by two transcripts that differ in the use of alternative 5′ coding exons, whereas p46Shc and p52Shc originate from different translation start sites in the same mRNA, such that p46Shc is an N-terminally truncated form of p52Shc (8). p52/p46Shc isoforms are scaffolds that associate with activated receptor tyrosine kinases (RTKs), and amplify signaling to the Ras-Erk MAP kinase and phosphatidylinositol 3′-kinase (PI3K)-Akt pathways. The p66Shc isoform emerged with vertebrates, and is characterized by an N-terminal collagen homology 2 (CH2) extension (9). p66Shc has been reported to promote oxidative stress and pro-apoptotic signaling in HeLa cells and murine embryonic fibroblasts (MEFs) (9-11). Unlike p52/p46, the abundance of p66Shc is substantially decreased in ErbB2 overexpressing breast cancer cell lines suggesting that p66Shc may function as an antagonist of p52/p46Shc, possibly acting as a tumor suppressor (12). Inactivation of p66Shc in mice improves glucose tolerance and insulin sensitivity (13, 14), and confers resistance to hyperglycemia-induced endothelial dysfunction (15). However, under nutrient stress conditions, mice lacking p66Shc are short-lived (16). These studies suggest that p66Shc may suppress metabolism by dampening growth factor signaling.

Using targeted mass spectrometry-based metabolomics, we have analyzed the effects of p66Shc on metabolic pathways. Our data suggests silencing of p66Shc improves glucose uptake, and redirects glucose carbon towards anabolic metabolism and increased cell size. In addition, we show that the effects of p66Shc are mediated, in part, through mTOR complexes 1 and 2 (mTORC1 and mTORC2, respectively). Our work reveals a role for p66Shc as an inhibitor of growth factor signalling and cell metabolism.

Results

Loss of p66Shc enhances glycolytic metabolism

To elucidate the involvement of p66Shc in cellular metabolism, we performed a targeted metabolomics analysis using liquid chromatography-tandem mass spectrometry (LC-MS/MS) in multiple reaction monitoring (MRM) mode. We measured ∼250 metabolites in positive or negative mode runs (table S1), and validated metabolite spectral patterns using standards. To assess the role of p66Shc in cancer cell metabolism, we initially used HeLa cells that were stably transfected with either a short hairpin shRNA that specifically targets the isoform p66Shc or a control hairpin (Fig. 1B) (17). When we analyzed the profiles of metabolites extracted from the two cell types, we noted that loss of p66Shc resulted in increased abundance of intermediates of glucose metabolism (Fig. 1C and fig. S1). Specifically, p66Shc deficiency was accompanied by significant increases in glucose-6-phosphate (G6P), and downstream glycolysis intermediates including fructose-6-bisphosphate (F6P), fructose-1,6-bisphosphate (F1,6BP), phosphoenolpyruvate (PEP), and pyruvate (Figure 1D). p66Shc-deficient HeLa cells produced more lactate than control cells, consistent with the Warburg effect. The metabolic shift also redirects glucose-derived citrate from the tricarboxylic acid cycle (TCA cycle) into lipid synthesis to generate biomass (18). Consistent with this effect, p66Shc-deficient cells had higher citrate concentrations (Fig. 1D). These data suggest that depletion of p66Shc is sufficient to enhance anabolic metabolism in HeLa cells.

Loss of p66Shc promotes glucose metabolism through the pentose phosphate and hexosamine biosynthesis pathways

In addition to the role of these molecules in glycolysis, G6P and F6P are precursors of the hexosamine biosynthesis and the pentose phosphate pathways, which are essential anabolic pathways in proliferating cells. The hexosamine biosynthesis pathway provides UDP-GlcNAc as a substrate for O-GlcNAcylation of cytosolic proteins, and N- and O-glycosylation of proteins produced in the secretory pathway. The pentose phosphate pathway provides ribose for nucleic acid synthesis and NADPH to maintain the reductive environment of the cell. In HeLa cells lacking p66Shc, we observed a ∼ 4-fold increase in N-acetylglucosamine-6-phosphate (GlcNAcP), and a ∼ 2-fold increase in UDP-GlcNAc abundance, the major products of the hexosamine biosynthesis pathway (Fig. 1E). A 2-3 fold increase in UDP-GlcNAc enhances N-glycosylation of growth factor receptors, thereby promoting positive feedback to signaling (19, 20). Concentrations of ribose-5-phosphate (R5P) and xylulose-5-phosphate (X5P) were also increased, which may involve the oxidative pentose phosphate pathway that contributes to redox balance (Fig. 1F).

Restoring p66Shc expression in p66Shc-deficient MEFs inhibits glycolytic metabolism

To test whether p66Shc was necessary for enhanced glycolytic metabolism, immortalized p66Shc KO MEFs were stably infected with either GFP or 3xFLAG-p66Shc retroviral vectors (hereafter referred to as KO and $p66^{+}$ *MEFs*, respectively) (Fig. 2A). Principal component analysis (PCA) was used to evaluate replicate consistency, and revealed a notable difference in the overall metabolic profiles of the p66Shc KO and $p66^{+}$ cells (fig. S2). Consistent with the p66Shc-mediated effects in HeLa cells, F6P and G6P were among

the metabolites with the most significant changes, and the abundance of glycolytic intermediates was generally lower in $p66^+$ MEFs compared to the KO cells (table 1). The abundance of glycolysis intermediates changed to a similar extent in MEFs as in HeLa cells; we observed ~ 3 fold decrease in G6P concentrations, and a concomitant decrease in downstream three-carbon glycolytic metabolites including PEP and lactate in $p66^+$ cells (Fig. 2B).

The lower concentration of citrate in $p66^+$ cells was accompanied by a concomitant decrease in the amounts of the fatty acid synthesis precursors acetyl-CoA and malonyl-CoA (Fig. 2C). Malonyl-CoA is a high energy and committed intermediate in fatty acid biosynthesis pathway, and is thus exclusively an anabolic metabolite. These results suggest that p66Shc inhibits *de novo* lipid biosynthesis. In addition, the abundance of intermediates in the hexosamine biosynthesis and pentose phosphate pathways was decreased in $p66^+$ MEFs (Fig. 2, D and E). This profile confirms that p66Shc deficiency in non-transformed cells enhanced glycolytic flux at the expense of decreasing oxidative mitochondrial metabolism. Indeed, p66Shc deficient MEFs displayed lower oxygen consumption (Fig. 2F) but improved energy utilization (AMP/ATP) (Fig. 2G).

p66Shc expression inhibits amino acid biosynthesis and pyrimidine metabolism

The difference in glucose uptake between p66Shc-deficient and p66Shc-competent MEFs was ~33% at most. However, the difference in the abundance of glycolytic metabolites ranged between 1.5- 3 fold. These results suggested a contribution from other nutrients such as amino acids that reversibly exchange with glycolytic intermediates. We detected higher amounts of non-essential amino acids, including alanine, serine and aspartate, in p66Shc-deficient MEFs (Fig. 3A). To determine whether the effect of p66Shc signaling on the steady state abundance of non-essential amino acids reflects regulation of metabolic flux through *de novo* synthesis, we measured the relative flux with a pulse of stable-isotope labeled ^{15}N-glutamine. Increased incorporation of labeled nitrogen into non-essential amino acids was detected in p66Shc KO MEFs (Fig. 3B). Increased flux of nitrogen from extracellular glutamine into non-essential amino acids in p66Shc KO MEFs is consistent with utilization catabolism of glutamine and reprograming that favors anabolism.

Pyrimidine derivatives (dCTP and UTP) were among the top 10 metabolites whose abundance was significantly decreased in $p66^+$ MEFs (Table 1). Pyrimidine nucleotides are required as high energy donors for phospholipid and glycoconjugate biosynthesis. $p66^+$ MEFs showed lower amounts of the pyrimidine synthesis intermediates orotate and dihydroorotate as compared to knockout MEFs (Fig. 3C). These results confirm that p66Shc inhibits anabolic metabolic pathways, and demonstrate a prominent role for p66Shc in reprogramming cell metabolism towards glucose catabolism and oxidative respiration.

p66Shc regulates redox homeostasis

By associating with cytochrome c, p66Shc promotes the generation of reactive oxygen species (ROS) (10, 21). Consistent with these findings, we observed a higher ratio of reduced to oxidized glutathione (GSH/GSSG) in p66Shc KO MEFs compared to $p66^+$ MEFs (Fig. 3D). The ratio of NADH/NAD^+ also reflects the redox state of the cell (22), and a ~ 3-

fold increase in NADH/NAD^+ indicates a more reducing environment in p66Shc-deficient cells (Fig. 3E). NADH is produced in the second half of glycolysis during the glyceraldehyde-3-phosphate dehydrogenase (GAPDH)-catalyzed step, and this may contribute to the altered NADH/NAD^+ ratio. The higher GSH/GSSG ratio in KO MEFs is consistent with the reported lower amounts of ROS in p66Shc KO MEFs (21). A previous report has shown that ROS contributes to insulin resistance and decreases glucose metabolism (23).

p66Shc is necessary and sufficient to alter glucose uptake and metabolism

To directly test whether p66Shc alters glucose uptake, we measured ^3H-labeled 2-deoxy glucose (2DG) uptake at different time points. The rate of 2DG uptake in p66Shc-deficient HeLa cells and in p66Shc KO MEFs was greater than in p66Shc-expressing cells (Fig. 4, A and B). Consistent with the enhanced glucose consumption and higher glycolytic metabolism in p66Shc-deficient cells we observed increased concentrations of extracellular lactate in the media of HeLa cells and MEFs lacking p66Shc (Fig. 4, C and D). However, Western blots showed no apparent difference in the abundance of glucose transporter 1 (GLUT1) between p66Shc-competent and p66Shc-deficient cells (fig. S3).

To monitor the effect of p66Shc on glucose catabolism, we examined the metabolites of ^{13}C-labeled glucose in control and p66Shc-deficient HeLa cells. The metabolism of [1,2-$^{13}C_2$] glucose generates M0, M1 and M2 mass isotopomers corresponding to ion fragments that contain zero, one or two labeled carbons, respectively (table S2). Rapid transfer of cells from unlabeled medium to identical medium containing [1,2-$^{13}C_2$]-labeled glucose ensures that metabolism is minimally disturbed (24). Consistent with enhanced glycolytic metabolism in p66Shc-depleted cells, the amounts of the M2-labeled form of G6P and downstream intermediates including M2 F6P and M2 pyruvate were increased in p66Shc-depleted HeLa cells (Fig. 4, F and G). p66Shc silencing enhanced the amount of labeled glucose-derived citrate and acetyl-CoA nearly 2 fold, consistent with the redirection of glucose-derived carbons towards lipid biosynthesis. Conversely, re-expressing p66Shc in p66Shc KO MEFs inhibited the increase in the abundance of [1,2-$^{13}C_2$] labeled glycolytic metabolites and downstream anabolic intermediates, including acetyl-CoA and citrate, in p66Shc-deficient cells (Fig. 4H). Additionally, p66Shc inhibited the *de novo* synthesis of amino acids (fig. S4). Collectively, our data suggest that p66Shc is necessary and sufficient to reprogram glucose utilization into anabolic pathways.

Lack of p66Shc enhances glycolytic flux and anabolic metabolism

To study the dynamics of incorporation of isotope-labeled glucose into downstream anabolic metabolites, we performed kinetics flux profiling in p66Shc KO and $p66^+$ MEFs using [1,2-$^{13}C_2$] labeled glucose by measuring the relative amounts of labeled glycolytic intermediates over 6 time points (0, 1, 2.5, 5, 10, 15 min). Consistent with the steady state data, we found that p66Shc inhibited labeled-glucose flux into glycolytic intermediates such as pyruvate in $p66^+$ MEFs (Fig. 5A). In addition, the amounts of labeled citrate, R5P and UDP-GlcNAc were lower in cells expressing p66Shc (Fig. 5, B-D). UDP-GlcNAc is a high-energy donor required for protein glycosylation and an example of an anabolic metabolite in which the GlcNAc portion is not catabolized back to glucose (20). Overall, these results

suggest that increased glycolytic flux in p66Shc-deficient cells accounts for the observed increase in metabolites at steady state, consistent with a role for p66Shc as an inhibitor of glucose catabolism.

p66Shc inhibits growth factor signaling to the metabolic sensor mTOR

Several aspects of the metabolic profile of p66Shc KO MEFs resemble that of cells with chronic mTOR activation; these include enhanced amounts of glycolytic and pentose phosphate pathway intermediates (G6P, F6P, and R5P) (25), increased amounts of *de novo* pyrimidine metabolites (26, 27), and increased lipid biosynthesis precursors (acetyl-CoA and malonyl-CoA) (25). To monitor mTOR signaling, we examined phosphorylation of Thr^{389} in the ribosomal protein S6 kinase (S6K1), a substrate of mTORC1, and Thr^{473} in Akt which is a direct target of mTORC2 (28). Following serum stimulation, p66Shc-deficient HeLa cells displayed markedly increased phosphorylation of both mTORC1 and mTORC2 targets compared to control cells, despite having equal abundance of the p52Shc and p46Shc isoforms (Fig. 6A). Similar results were obtained with insulin stimulation (Fig. 6B). Pre-treatment of cells with the mTOR inhibitor Torin1 (29) abolished the phosphorylation of mTOR targets in both cell types confirming the specificity of the signal (Fig. 6A and 6B). We also found that amino acid activation of the mTORC1 pathway was enhanced in p66Shc-deficient HeLa cells (fig. S5A). In $p66^{+}$ MEFs, p66Shc inhibited the activation of mTOR targets following stimulation with IGF-1 and insulin, but not with EGF (Fig. 6C). This observation is consistent with previous reports showing that p66Shc has little effect on EGF signaling (9). The phosphorylation of mTORC1 and mTORC2 targets was decreased in $p66^{+}$ MEFs following serum (Fig. 6D) and amino acid stimulation (Fig. S5B). In contrast to the inhibitory effects of p66Shc expression on mTOR signaling in KO MEFs, mTOR activation was sustained in KO MEFs stably overexpressing the p52Shc isoform (Fig. 6E). This confirms earlier reports that the p66Shc and p52Shc isoforms have opposing effects attributable to the unique N-terminal CH2 region of p66Shc (9, 30).

Loss of p66Shc causes an increase in cell size

mTOR functions as a central regulator of cell growth (31). The inhibitory effect of p66Shc on mTOR activation therefore predicted that p66Shc deficiency would lead to a larger cell size. Indeed, stable re-expression of p66Shc in p66Shc KO MEFs caused a decrease in cell size as measured by FACS forward scatter analysis (Fig. 6F). These findings were confirmed using coulter counter measurement (fig. S6A). Conversely, HeLa cells depleted of p66Shc displayed an increase in median cell size, consistent with redirection of glucose-derived carbon towards biomass synthesis (fig. S6B). Together, these results suggest that p66Shc acts as a negative regulator of the nutrient-sensing mTOR signaling pathway leading to inhibition of cell growth and anabolic metabolism.

Effects of p66Shc on glycolytic metabolism are mediated through mTOR

To determine which mTOR complex contributes to the metabolic phenotype observed in p66Shc null cells, we treated p66Shc KO and $p66^{+}$ MEFs with rapamycin for 16 h, a time frame that inhibits both mTORC1 and mTORC2 enzymes (Fig. 7A). In line with reports linking mTORC1 and mTORC2 to glycolytic metabolism (25, 32, 33), we found that

inhibition of both mTOR complexes partly reversed the metabolic phenotype of p66Shc KO MEFs, notably diminishing the increase in the hexosamine biosynthesis pathway (UDP-GlcNAc) and the pentose phosphate pathway (R5P) (Fig. 7B). A similar trend was observed in *de novo* pyrimidine synthesis (Fig. 7C). Furthermore, inhibition of Akt, a kinase that is upstream of mTORC1 and downstream of mTORC2 (28), significantly decreased the amounts of glycolytic metabolites in p66Shc-deficient MEFs (fig. S7).

p66Shc alters gene expression

To understand how p66Shc signals to mTORC1 and mTORC2, we attempted to find unique p66Shc binding partners by mass spectrometry. However, all proteins that bound to p66Shc in our experiments have also been reported to bind to p52Shc following serum stimulation (table S4) (34). The steady-state condition of p66Shc KO and $p66^{+}$ MEFs is likely to include differences in gene expression. To address this question, we performed RNA-seq analysis comparing the expression profile of p66Shc KO and $p66^{+}$ MEFs. Our data shows significant differences in the expression of $\sim$ 400 genes but not for genes encoding glycolytic enzymes, including hexokinase and phosphofructokinase, or those encoding glucose transporters (table S3). This suggests that changes in steady-state abundance of p66Shc regulates metabolism largely through signaling and posttranslational modification.

Discussion

Our results provide evidence that p66Shc expression is associated with dampened signaling response to insulin stimulation and reduced glycolytic metabolism. Hyperglycemia has been previously shown to induce p66Shc expression (35). Our data suggests that p66Shc mediates feedback inhibition of growth signaling and glucose metabolism in cells (Fig. 7D). For metabolites that are intermediates in both catabolic and anabolic directions, the delivery of ^{13}C-labeled glucose reveals competing delivery from cold sources including storage products, autophagy and uptake of other nutrients. For central metabolites such as pyruvate, citrate, R5P and UDP-GlcNAc, our flux analysis show faster ^{13}C incorporation and an increase to a higher steady state in p66Shc-deficient cells, indicating a larger contribution from ^{13}C-glucose than the non-radioactive sources in cells lacking p66Shc.

Furthermore, p66Shc deficiency in mice improves glucose tolerance and insulin sensitivity (13, 14). p66Shc silencing in both transformed and non-transformed immortalized cells improves glucose uptake, increases lactate production, and metabolite abundance for fatty acid biosynthesis, the hexosamine pathway, pentose phosphate pathway and amino acids contributing to increased cell size. This metabolic shift depends in part on the mTOR pathway, because rapamycin treatment reversed the glycolytic shift caused by p66Shc loss (Fig. 4D). These effects are particularly striking because the p52Shc isoform is identical to p66Shc in all but the N-terminal CH2 region, and has the opposing function of promoting the activation of the Ras-Erk and PI3K-Akt pathways. p66Shc acts as an inhibitor of mTORC1 and mTORC2 signaling, pathways that support protein synthesis associated with increased cell size. mTOR inhibition reduced anabolic metabolites partially restoring the p66Shc-competent phenotype, suggesting that mTOR-independent pathways also contribute to p66Shc-deficiency phenotype. p66Shc expression has been inversely correlated to

tumorigenesis (12), which is consist with our results in which p66Shc loss enhances mTOR signaling and anabolic metabolism. It is possible that p66Shc competes with p52Shc for binding partners in a dynamic manner that disrupts downstream signaling to mTOR. Time courses for receptor recruitment of signaling complexes may reveal the molecular basis for p66Shc action on signaling and anabolic metabolism.

RNA-seq analysis showed no differences in expression of genes encoding metabolic enzymes and glucose transporters between p66Shc-competent and p66Shc-deficient cells. Transcripts showing a chance in abundance were clustered in the category of secretory proteins, and additional studies are required to assess their contribution to the p66Shc phenotype. Rapid forms of regulation such as allostery and posttranslational modifications to metabolic enzymes and transporters may account for much of the observed p66Shc-depdendent metabolic reprogramming. However, on a longer time scale, the stable cell lines used in our experiments have adapted to p66Shc expression or loss, and the attendant changes in signaling and metabolism flux may be reinforced by some of the changes in gene expression.

In summary, our results indicate that the Shc1 locus not only regulates mitogenic signaling, but also modifies anabolic metabolism in an mTOR-dependent manner. Our data points to the prospect that monitoring or modulating p66Shc abundance could be important in the management of pathological conditions in which metabolic signaling is dysregulated, such as cancer and diabetes.

Materials and Methods

Reagents were obtained from the following sources: antibodies to phospho-Thr^{389} S6K1, phosho-Thr^{308} Akt, phospho-Ser^{473} Akt, Akt, and S6K1 from Cell Signaling Technology; mouse and rabbit Shc1 antibodies from BD transduction laboratories; FLAG and tubulin antibodies, amino acids, insulin, IGF-1, and EGF from Sigma-Aldrich; FuGENE 6, Complete Protease Cocktail from Roche; rapamycin from LC laboratories, DMEM from Gibco; Inactivated Fetal Calf Serum (IFS) from Hyclone, amino acid-free RPMI from US Biological; BCA assay reagent, protein G-sepharose from Pierce; Akt Inhibitor IV (EMD4Biosciences).

Cell lines and tissue culture

HeLa and MEFs were cultured in DMEM with 10% IFS and penicillin/streptomycin. p66Shc KO MEFs were kindly provided by P.G. Pelicci (IFOM). 3xFLAG-p66Shc expressing MEFs were generated by retroviral infection of gateway-compatible pMX vector with murine p66Shc cDNA. Stably infected cells were maintained under 1 μg/ml puromycin selection. For stable p66Shc knockdown in HeLa cells, we used the following hairpin sequence:

sense 5′-cgg aat gag tct ctg tca tcg ct (tt)-3′ and anti-sense 5′-ag cga tga cag aga ctc att ccg (tt)-3′

Amino acid stimulation

Almost confluent cultures in 6-well culture plates were rinsed with amino acid-free RPMI once, incubated in amino acid-free RPMI for 50 minutes, and stimulated with 52 μg/ml leucine for 10 minutes. For amino acid starvation, cells in 10 cm culture dishes or coated glass cover slips were rinsed with and incubated in amino acid-free RPMI for 50 minutes, and stimulated with a 10× amino acid mixture for 10 minutes as indicated in the figures. Following stimulation, the final concentration of amino acids in the media was the same as in RPMI. The 10× amino acid mixture was prepared from individual amino acid powders.

Cell lysis and Western blots

Cells were rinsed once with ice-cold PBS and lysed in ice-cold lysis buffer (40 mM HEPES [pH 7.4], 2 mM EDTA, 10 mM pyrophosphate, 10 mM glycerophosphate, and 0.5% NP-40, and one tablet of EDTA-free protease inhibitors (Roche) per 10 ml). The soluble fractions of cell lysates were isolated by centrifugation at 13,000 rpm for 10 minutes by centrifugation in a microfuge. Proteins were denatured by the addition of 2× sample buffer and boiling for 5 minutes, resolved by 8% SDS-PAGE, and analyzed by immunoblotting for the indicated proteins in the figures.

Metabolomic profiling

The relative abundance of metabolites were determined in HeLa cells and MEFs using the following protocol (36): Cells were seeded in 6-well plate in replicates. After 24 h, the media were removed and the cells were washed 2-times with warm PBS, then the cells were placed on dry ice. The metabolites were immediately extracted by adding 1 mLof extraction solution (40% acetonitrile, 40% methanol, and 20% water) containing internal standards (500μg/ml and 300μg/ml of D7-Glucose and 13C915N-Tyrosine, respectively) and then the cells were scraped and collected in 1.5 mL vials. The mixture was shaken for 1 hr at 4°C and 1400 rpm in a Thermomixer (Eppendorf, Germany). The samples were spun down at 14000 rpm, for 10 min at 4°C (Eppendorf, Germany), and supernatants were transferred into fresh tubes to be evaporated to dryness in a CentreVap concentrator at 40°C (Labconco, MO). The dry extract samples were stored at -80°C until LC/MS analysis. The dry metabolite extracts were reconstituted in 100μL of water. For positive and negative mode analysis, sample was injected twice through reversed phase column an Inertsil ODS-3, 4.6 mm internal diameter, 150 mm length, and 3 μM particle size (Dionex Corporation, CA).). In positive mode analysis, where the mobile phase gradient ramps from 5% to 90% of acetonitrile in 16 min, after 1 min at 90%, the composition returns to 5% acetonitrile in 0.1% acetic acid in two min. In negative mode, where the acetonitrile composition ramped from 5 to 90% in 10 min, after 1 min at 90%, the gradient returns to 5% acetonitrile in buffer-A (0.1% tributylamine, 0.03% acetic acid, 15% methanol). The total runtime in both modes was 20 min, the samples were stored at 4°C, and the injection volume was 10 μL. An automated washing procedure was developed before and after each sample to avoid any sample carryover.

The eluted metabolites were analyzed at the optimum polarity in MRM mode on electrospray ionization (ESI) triple-quadrupole mass spectrometer (ABSciex4000Qtrap, Toronto, ON, Canada). The mass spectrometric data acquisition time for each run is 20 min, and the dwell time for each MRM channel is 10 ms. Common mass spectrometric

parameters are the same as tuning conditions described above, except: GS1 and GS2 were 50 psi; CUR was 20 psi, and CAD was 3 and 7 for positive and negative modes, respectively, and source temperature (TEM) was 400°C. Signal was normalized to internal standard and cell number. Metaboanalyst was used to analyze the data (37). The LC-MS/MS system does not resolve hexose and hexoseamine isomers including glucose/galactose and GlcNAc/GalNAc. To monitor trends in metabolic pathways, we referred to these isomers in their glucose (Glc) forms.

Statistics

Unpaired two-tailed Student's t-tests were performed comparing two groups. For multiple comparisons analysis, we used one-way ANOVA followed by Bonferroni's *post hoc* test. All experiments represent at least three biological replicates.

[^{3}H]-2-deoxy-d-glucose uptake assay

MEF and HeLa cells grown in 6-well plates were rinsed with HEPES-buffered saline [140 mM NaCl, 20 mM HEPES, 5 mM KCl, 2.5 mM MgSO4, 1 mM CaCl2 (pH 7.4)]. 2-DG uptake was performed for 3, 5, and 10 min in HEPES-buffered saline containing 2 mM unlabeled 2-DG and 0.2 μCi/ml 2-[3H] DG at room temperature. The reaction was terminated by washing three times in ice-cold 0.9% NaCl (w/v). To quantify the radioactivity incorporated, cells were lysed with 0.05 N NaOH and lysates were counted with scintillation fluid in a β-counter. Nonspecific uptake was determined in the presence of cytochalasin B (10 μM) during the assay. The results are expressed as pmole 2-DG transported per min/mg of protein.

Oxygen consumption rate measurement

Cells were seeded at 50,000 cells/well in XF-24 cell culture plates. The day after the seeding, cell culture media was replaced with unbuffered RPMI and oxygen consumption was measured using an XF-24 Flux Analyzer as described in (38).

Isotope labeling and kinetic profiling

Media of cell cultures in 6-well dishes were replaced with unlabeled fresh DMEM 2h before exposure to labeled glucose. The media was then replaced with DMEM containing 25 mM [1,2-$^{13}C_2$]-labeled glucose or ^{15}N-labeled glutamine for the times indicated in the figures legends (Cambridge Isotope Laboratories). Metabolites were extracted and analyzed as mentioned in the Metabolomics profiling section using different MRM transitions that were developed for 1,2 ^{13}C-glucose as detailed in table S1.

Mass spectrometry analysis of the p66Shc protein-interactions

The p66Shc protein interaction network was determined following a protocol described in (34). p66$^+$ MEFs were washed three times with ice-cold PBS and lysed in NP40 lysis buffer (50 mM HEPES-NaOH, pH 8, 150 mM NaCl, 1 mM EGTA, 0.5% NP40, 100 mM NaF, 2.5 mM MgCl2, 10mM Na4P2O7, 1 mM DTT, 10% glycerol) supplemented with protease and phosphatase inhibitors (50 mM β-glycerolphosphate, 10μgml–1 aprotinin, 10μgml–1 leupeptin, 1 mM Na3VO4, 100 nM calyculin A, 1 mM PMSF (phenylmethylsulphonyl

fluoride)). The total cell lysates were centrifuged at 10,000 rpm for 15 min to pellet nuclei and insoluble material. Nuclear-free lysates were pre-cleared by one-hour incubation with protein A sepharose and normalized for total protein concentration using the Bio-Rad protein assay. 3x-FLAG-p66Shc was immunoprecipitated by incubating lysates with 5 μl (bed volume) anti-Flag M2 antibody-conjugated agarose for 4 h at 4 °C.

RNA-seq

cDNA library preparation using Illumina TruSeq RNA Sample Prep Kit v2 (Cat#RS-122-2001). Briefly, 1 μg of high quality total RNA were isolated from p66Shc KO and $p66^{+}$ MEFs to generate the cDNA library according to the Illunima's protocol. The generated barcoded cDNA library has an average fragment size of 350-400 bp. This bar-coded library is quality checked with Agilent Bioanalyzer and quantified with qPCR using KAPA SYBR FAST Universal 2× qPCR Master Mix (Kapa Biosystem, Cat#KK4602). The quality checked libraries are then loaded on a flowcell for cluster generation using Illumina c-Bot and TruSeq PE Cluster Kit v3 (Cat#: PE-401-3001). Sequencing was done on HiSeq2000 with TruSeq SBS Kit v3 (pair-ended 200 cycles, Cat#: FC401-3001). The real-time base call (.bcl) files are converted to fastq files using CASAVA 1.8.2 (on CentOS 6.0 data storage and computation linux servers).

Supplementary Material

Refer to Web version on PubMed Central for supplementary material.

Acknowledgments

The authors dedicate the manuscript in memory of Dr. Tony Pawson who passed away during the revision process. The research was supported by grants from Genome Canada through the OGI, and funding from Ontario Research Fund Global Leadership Round in Genomics & Life Sciences (ORF-GL2) and Canadian Cancer Society to TP and JWD. JWD is also supported by grants from CIHR (MOP-62975), Sydney C. Cooper Program, and the Canada Research Chairs Program. The authors are indebted to P.G. Pelicci and G. Cortopassi for providing p66Shc null and control MEFs and K. Chan and C.Y. Ho for performing the RNA-seq experiments. We thank M. Stacey and K. Riabowol for critical reading of the manuscript, as well as J. Gish and J. Woodgett for their encouragement and insight.

Funding: D.M.S is supported by grants from the NIH, Department of Defense, and awards from the Keck and LAM Foundation. D.W.L is supported by Ruth Kirschstein National Research Service and NIH K99 Awards. D.M.S. is an investigator of Howard Hughes Medical Institute. M.A.S is supported by a Vanier Canada and Ontario Graduate Studentships.

References

1. Scott JD, Pawson T. Cell signaling in space and time: where proteins come together and when they're apart. Science. 2009; 326:1220–1224. [PubMed: 19965465]
2. Hsu PP, Kang SA, Rameseder J, Zhang Y, Ottina KA, Lim D, Peterson TR, Choi Y, Gray NS, Yaffe MB, Marto JA, Sabatini DM. The mTOR-regulated phosphoproteome reveals a mechanism of mTORC1-mediated inhibition of growth factor signaling. Science. 2011; 332:1317–1322. [PubMed: 21659604]
3. Yu Y, Yoon SO, Poulogiannis G, Yang Q, Ma XM, Villen J, Kubica N, Hoffman GR, Cantley LC, Gygi SP, Blenis J. Phosphoproteomic analysis identifies Grb10 as an mTORC1 substrate that negatively regulates insulin signaling. Science. 2011; 332:1322–1326. [PubMed: 21659605]

4. Wang L, Balas B, Christ-Roberts CY, Kim RY, Ramos FJ, Kikani CK, Li C, Deng C, Reyna S, Musi N, Dong LQ, DeFronzo RA, Liu F. Peripheral disruption of the Grb10 gene enhances insulin signaling and sensitivity in vivo. Mol Cell Biol. 2007; 27:6497–6505. [PubMed: 17620412]
5. Smith FM, Holt LJ, Garfield AS, Charalambous M, Koumanov F, Perry M, Bazzani R, Sheardown SA, Hegarty BD, Lyons RJ, Cooney GJ, Daly RJ, Ward A. Mice with a disruption of the imprinted Grb10 gene exhibit altered body composition, glucose homeostasis, and insulin signaling during postnatal life. Mol Cell Biol. 2007; 27:5871–5886. [PubMed: 17562854]
6. Vander Heiden MG, Cantley LC, Thompson CB. Understanding the Warburg effect: the metabolic requirements of cell proliferation. Science. 2009; 324:1029–1033. [PubMed: 19460998]
7. Hanahan D, Weinberg RA. Hallmarks of cancer: the next generation. Cell. 2011; 144:646–674. [PubMed: 21376230]
8. Pelicci G, Lanfrancone L, Grignani F, McGlade J, Cavallo F, Forni G, Nicoletti I, Pawson T, Pelicci PG. A novel transforming protein (SHC) with an SH2 domain is implicated in mitogenic signal transduction. Cell. 1992; 70:93–104. [PubMed: 1623525]
9. Migliaccio E, Mele S, Salcini AE, Pelicci G, Lai KM, Superti-Furga G, Pawson T, Di Fiore PP, Lanfrancone L, Pelicci PG. Opposite effects of the p52shc/p46shc and p66shc splicing isoforms on the EGF receptor-MAP kinase-fos signalling pathway. EMBO J. 1997; 16:706–716. [PubMed: 9049300]
10. Pinton P, Rimessi A, Marchi S, Orsini F, Migliaccio E, Giorgio M, Contursi C, Minucci S, Mantovani F, Wieckowski MR, Del SG, Pelicci PG, Rizzuto R. Protein kinase C beta and prolyl isomerase 1 regulate mitochondrial effects of the life-span determinant p66Shc. Science. 2007; 315:659–663. [PubMed: 17272725]
11. Migliaccio E, Giorgio M, Mele S, Pelicci G, Reboldi P, Pandolfi PP, Lanfrancone L, Pelicci PG. The p66shc adaptor protein controls oxidative stress response and life span in mammals. Nature. 1999; 402:309–313. [PubMed: 10580504]
12. Stevenson LE, Frackelton AR Jr. Constitutively tyrosine phosphorylated p52 Shc in breast cancer cells: correlation with ErbB2 and p66 Shc expression. Breast Cancer Res Treat. 1998; 49:119–128. [PubMed: 9696394]
13. Ranieri SC, Fusco S, Panieri E, Labate V, Mele M, Tesori V, Ferrara AM, Maulucci G, De SM, Martorana GE, Galeotti T, Pani G. Mammalian life-span determinant p66shcA mediates obesity-induced insulin resistance. Proc Natl Acad Sci U S A. 2010; 107:13420–13425. [PubMed: 20624962]
14. Tomilov AA, Ramsey JJ, Hagopian K, Giorgio M, Kim KM, Lam A, Migliaccio E, Lloyd KC, Berniakovich I, Prolla TA, Pelicci P, Cortopassi GA. The Shc locus regulates insulin signaling and adiposity in mammals. Aging Cell. 2011; 10:55–65. [PubMed: 21040401]
15. Camici GG, Schiavoni M, Francia P, Bachschmid M, Martin-Padura I, Hersberger M, Tanner FC, Pelicci P, Volpe M, Anversa P, Luscher TF, Cosentino F. Genetic deletion of p66(Shc) adaptor protein prevents hyperglycemia-induced endothelial dysfunction and oxidative stress. Proc Natl Acad Sci U S A. 2007; 104:5217–5222. [PubMed: 17360381]
16. Giorgio M, Berry A, Berniakovich I, Poletaeva I, Trinei M, Stendardo M, Hagopian K, Ramsey JJ, Cortopassi G, Migliaccio E, Notzli S, Amrein I, Lipp HP, Cirulli F, Pelicci PG. The p66Shc knocked out mice are short lived under natural condition. Aging Cell. 2012; 11:162–168. [PubMed: 22081964]
17. Kisielow M, Kleiner S, Nagasawa M, Faisal A, Nagamine Y. Isoform-specific knockdown and expression of adaptor protein ShcA using small interfering RNA. Biochem J. 2002; 363:1–5. [PubMed: 11903040]
18. Hatzivassiliou G, Zhao F, Bauer DE, Andreadis C, Shaw AN, Dhanak D, Hingorani SR, Tuveson DA, Thompson CB. ATP citrate lyase inhibition can suppress tumor cell growth. Cancer Cell. 2005; 8:311–321. [PubMed: 16226706]
19. Lau KS, Partridge EA, Grigorian A, Silvescu CI, Reinhold VN, Demetriou M, Dennis JW. Complex N-glycan number and degree of branching cooperate to regulate cell proliferation and differentiation. Cell. 2007; 129:123–134. [PubMed: 17418791]

20. Wellen KE, Lu C, Mancuso A, Lemons JM, Ryczko M, Dennis JW, Rabinowitz JD, Coller HA, Thompson CB. The hexosamine biosynthetic pathway couples growth factor-induced glutamine uptake to glucose metabolism. Genes Dev. 2010; 24:2784–2799. [PubMed: 21106670]
21. Giorgio M, Migliaccio E, Orsini F, Paolucci D, Moroni M, Contursi C, Pelliccia G, Luzi L, Minucci S, Marcaccio M, Pinton P, Rizzuto R, Bernardi P, Paolucci F, Pelicci PG. Electron transfer between cytochrome c and p66Shc generates reactive oxygen species that trigger mitochondrial apoptosis. Cell. 2005; 122:221–233. [PubMed: 16051147]
22. Fisher-Wellman KH, Neufer PD. Linking mitochondrial bioenergetics to insulin resistance via redox biology. Trends Endocrinol Metab. 2012; 23:142–153. [PubMed: 22305519]
23. Houstis N, Rosen ED, Lander ES. Reactive oxygen species have a causal role in multiple forms of insulin resistance. Nature. 2006; 440:944–948. [PubMed: 16612386]
24. Munger J, Bennett BD, Parikh A, Feng XJ, McArdle J, Rabitz HA, Shenk T, Rabinowitz JD. Systems-level metabolic flux profiling identifies fatty acid synthesis as a target for antiviral therapy. Nat Biotechnol. 2008; 26:1179–1186. [PubMed: 18820684]
25. Duvel K, Yecies JL, Menon S, Raman P, Lipovsky AI, Souza AL, Triantafellow E, Ma Q, Gorski R, Cleaver S, Vander Heiden MG, MacKeigan JP, Finan PM, Clish CB, Murphy LO, Manning BD. Activation of a metabolic gene regulatory network downstream of mTOR complex 1. Mol Cell. 2010; 39:171–183. [PubMed: 20670887]
26. Ben-Sahra I, Howell JJ, Asara JM, Manning BD. Stimulation of de Novo Pyrimidine Synthesis by Growth Signaling Through mTOR and S6K1. Science. 2013; 339:1323–1328. [PubMed: 23429703]
27. Robitaille AM, Christen S, Shimobayashi M, Cornu M, Fava LL, Moes S, Prescianotto-Baschong C, Sauer U, Jenoe P, Hall MN. Quantitative Phosphoproteomics Reveal mTORC1 Activates de Novo Pyrimidine Synthesis. Science. 2013; 339:1320–1323. [PubMed: 23429704]
28. Zoncu R, Efeyan A, Sabatini DM. mTOR: from growth signal integration to cancer, diabetes and ageing. Nat Rev Mol Cell Biol. 2011; 12:21–35. [PubMed: 21157483]
29. Thoreen CC, Kang SA, Chang JW, Liu Q, Zhang J, Gao Y, Reichling LJ, Sim T, Sabatini DM, Gray NS. An ATP-competitive mammalian target of rapamycin inhibitor reveals rapamycin-resistant functions of mTORC1. J Biol Chem. 2009; 284:8023–8032. [PubMed: 19150980]
30. Xi G, Shen X, Clemmons DR. p66shc negatively regulates insulin-like growth factor I signal transduction via inhibition of p52shc binding to Src homology 2 domain-containing protein tyrosine phosphatase substrate-1 leading to impaired growth factor receptor-bound protein-2 membrane recruitment. Mol Endocrinol. 2008; 22:2162–2175. [PubMed: 18606861]
31. Wullschleger S, Loewith R, Hall MN. TOR signaling in growth and metabolism. Cell. 2006; 124:471–484. [PubMed: 16469695]
32. Hagiwara A, Cornu M, Cybulski N, Polak P, Betz C, Trapani F, Terracciano L, Heim MH, Ruegg MA, Hall MN. Hepatic mTORC2 activates glycolysis and lipogenesis through Akt, glucokinase, and SREBP1c. Cell Metab. 2012; 15:725–738. [PubMed: 22521878]
33. Lamming DW, Demirkan G, Boylan JM, Mihaylova MM, Peng T, Ferreira J, Neretti N, Salomon A, Sabatini DM, Gruppuso PA. Hepatic signaling by the mechanistic target of rapamycin complex 2 (mTORC2). FASEB journal : official publication of the Federation of American Societies for Experimental Biology. 2014; 28:300–315. published online EpubJan. 10.1096/fj.13-237743 [PubMed: 24072782]
34. Zheng Y, Zhang C, Croucher DR, Soliman MA, St-Denis N, Pasculescu A, Taylor L, Tate SA, Hardy WR, Colwill K, Dai AY, Bagshaw R, Dennis JW, Gingras AC, Daly RJ, Pawson T. Temporal regulation of EGF signalling networks by the scaffold protein Shc1. Nature. 2013; 499:166–171. published online EpubJul 11. 10.1038/nature12308 [PubMed: 23846654]
35. Xi G, Shen X, Radhakrishnan Y, Maile L, Clemmons D. Hyperglycemia-Induced p66shc Inhibits Insulin-Like Growth Factor I-Dependent Cell Survival via Impairment of Src Kinase-Mediated Phosphoinositide-3 Kinase/AKT Activation in Vascular Smooth Muscle Cells. Endocrinology. 2010
36. Abdel Rahman AM, Ryczko J, Pawling J, Dennis JW. Probing the hexosamine biosynthetic pathway in human tumor cells by multitargeted tandem mass spectrometry. ACS chemical

biology. 2013; 8:2053–2062. published online EpubSep 20. 10.1021/cb4004173 [PubMed: 23875632]

37. Xia J, Wishart DS. Web-based inference of biological patterns, functions and pathways from metabolomic data using MetaboAnalyst. Nat Protoc. 2011; 6:743–760. [PubMed: 21637195]
38. Birsoy K, Wang T, Possemato R, Yilmaz OH, Koch CE, Chen WW, Hutchins AW, Gultekin Y, Peterson TR, Carette JE, Brummelkamp TR, Clish CB, Sabatini DM. MCT1-mediated transport of a toxic molecule is an effective strategy for targeting glycolytic tumors. Nature genetics. 2013; 45:104–108. published online EpubJan. doi:110.1038/ng.2471. [PubMed: 23202129]

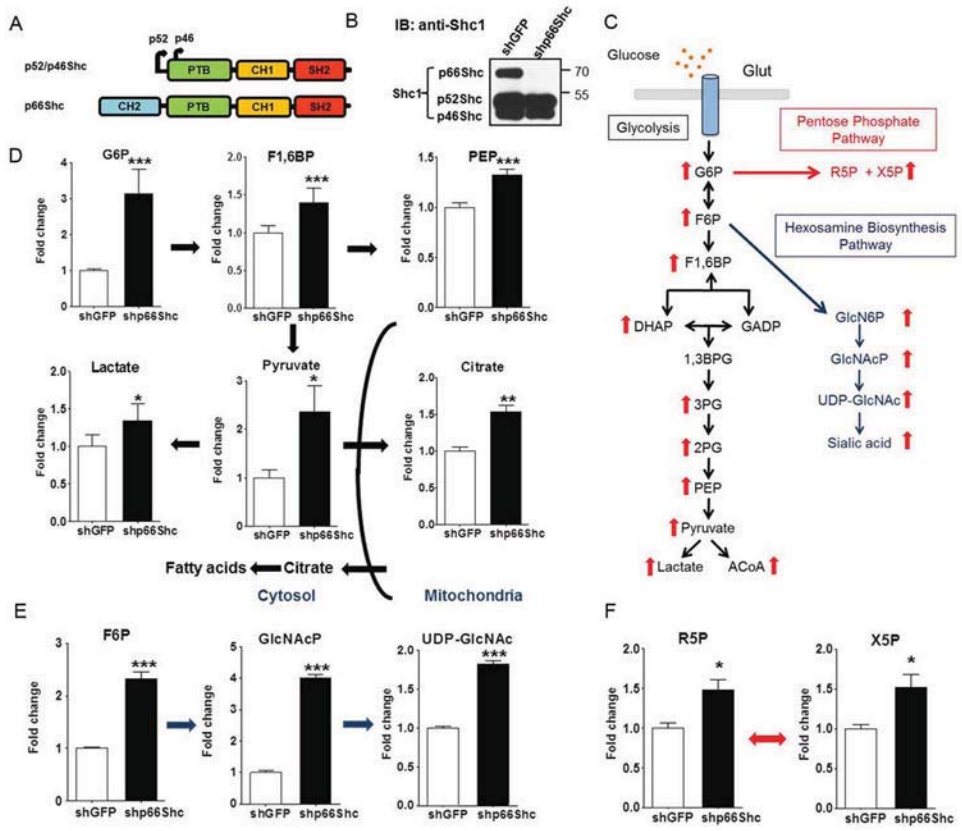

Fig. 1. p66Shc deficiency enhances glycolytic metabolism and causes a Warburg shift

(A) Diagram of the three isoforms of mammalian Shc1. (B) Abundance of the three Shc1 isoforms in HeLa cells stably expressing shRNAs targeting GFP or p66Shc. N = 3 biological replicates. (C) Summary of the changes in intracellular metabolite amounts associated with p66Shc knockdown in HeLa cells analyzed by LC-MS/MS. (D-F) Fold change of glycolytic (D), hexosamine biosynthesis pathway (E), and pentose phosphate pathway (F) intermediates in p66Shc-deficient and p66Shc-competent HeLa cells as measured by LC-MS/MS. Glucose-6-phosphate (G6P); Fructose-1,6-phosphate (F1,6BP); Phosphoenolpyruvate (PEP), Fructose-6-phosphate (F6P); N-acetylglucosamine phosphate (GlcNAcP); Uridine diphosphate N-acetylglucosamine (UDP-GlcNAc), ribose-5-phosphate (R5P) and xylulose-5-phosphate (X5P). Error bars represent SD of three biological replicates (* $p < 0.05$, ** $p < 0.01$, *** $p < 0.001$).

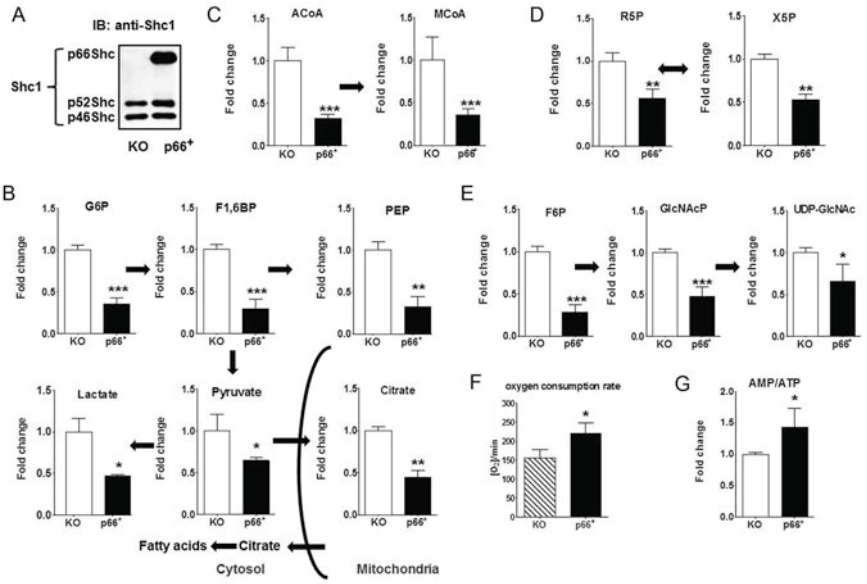

Fig. 2. Rescue of p66Shc expression in p66Shc KO MEF (p66^{+} cells) inhibits glycolytic metabolism in favour of oxidative metabolism

(A) Abundance of the three Shc1 isoforms in p66Shc KO MEFs stably infected with GFP (KO) or FLAG-p66Shc (p66^{+}). N = 3 biological replicates. (B-E) p66Shc expression inhibits glycolytic metabolism. Data represents fold change of glycolytic intermediates (B), acetyl-CoA (ACoA) and malonyl-CoA (MCoA) (C), pentose phosphate pathway intermediates (D), and hexosamine biosynthesis pathway intermediates (E) in p66Shc-deficient (white) and p66Shc-competent (black) MEFs as measured by LC-MS/MS. (G) p66Shc deficiency inhibits oxygen consumption rate as measured by XF-24 Flux Analyzer. (H) Relative amounts of AMP/ATP ratio in p66Shc KO and p66^{+} MEFs by LC-MS/MS. In all experiments, error bars represent SD of at least three biological replicates (* $p < 0.05$, ** $p < 0.01$, *** $p < 0.001$).

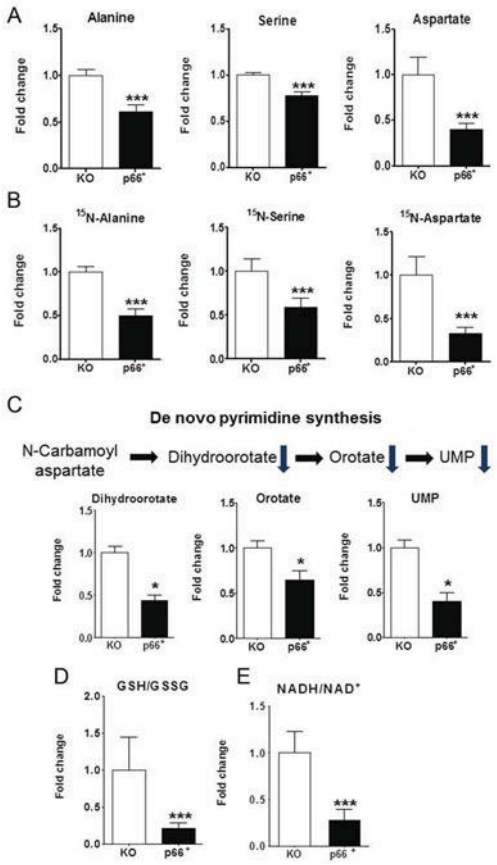

Fig. 3. p66Shc expression inhibits the biosynthesis of amino acids and pyrimidines and regulates redox homeostasis

(A) Fold change of steady state alanine, serine and aspartate, measured by LC-MS/MS. (B) Fold change of intracellular amounts of ^{15}N-labeled alanine, serine and aspartate in p66Shc KO and p66^{+} cells grown in media containing ^{15}N-glutamine for 2h. (C) Fold change of *de novo* pyrimidine synthesis intermediates, N-carbamoyl aspartate, orotate and UMP. (D and E) Relative amounts of the ratio of reduced/oxidized glutathione (GSH/GSSG) (D), and reduced/oxidized NAD^{+} (NADH/NAD^{+}) (E) in p66Shc KO and p66^{+} MEFs. In all experiments, error bars represent SD of at least three biological replicates (* $p < 0.05$, *** $p < 0.001$).

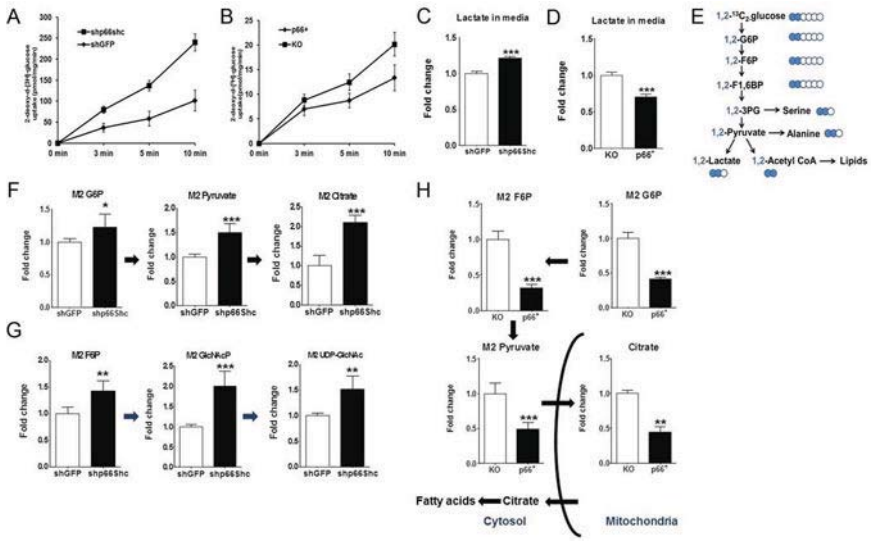

Fig. 4. p66Shc is necessary and sufficient to alter glucose uptake and glycolytic metabolism

(A and B) Tracing of ^{3}H-labeled 2-deoxy glucose (2DG) uptake over time in p66Shc-competent and p66Shc-deficient HeLa cells stably expressing shRNAs targeting GFP (A) or p66Shc and p66Shc KO and p66^{+} MEFs (B). (C and D) Fold change of extracellular lactate in media from p66Shc-competent and p66Shc-deficient HeLa (C) and MEFs (D). (E) Schematic diagram of ^{13}C-labeling patterns of metabolic products with [1,2-$^{13}C_2$] labeled glucose as a tracer. Blue circles indicate ^{13}C-labeled carbons. (F-G) Fold change of ^{13}C-labeled glycolytic (F), hexosamine biosynthesis pathway (G) intermediates in p66Shc-competent (white) and p66Shc-deficient cells (black) HeLa cells. (H) ^{13}C-labeled glycolytic intermediates in p66Shc KO (white) and p66^{+} (black) MEFs. Error bars represent SD of at least three independently prepared samples (* $p < 0.05$, ** $p < 0.01$, *** $p < 0.001$).

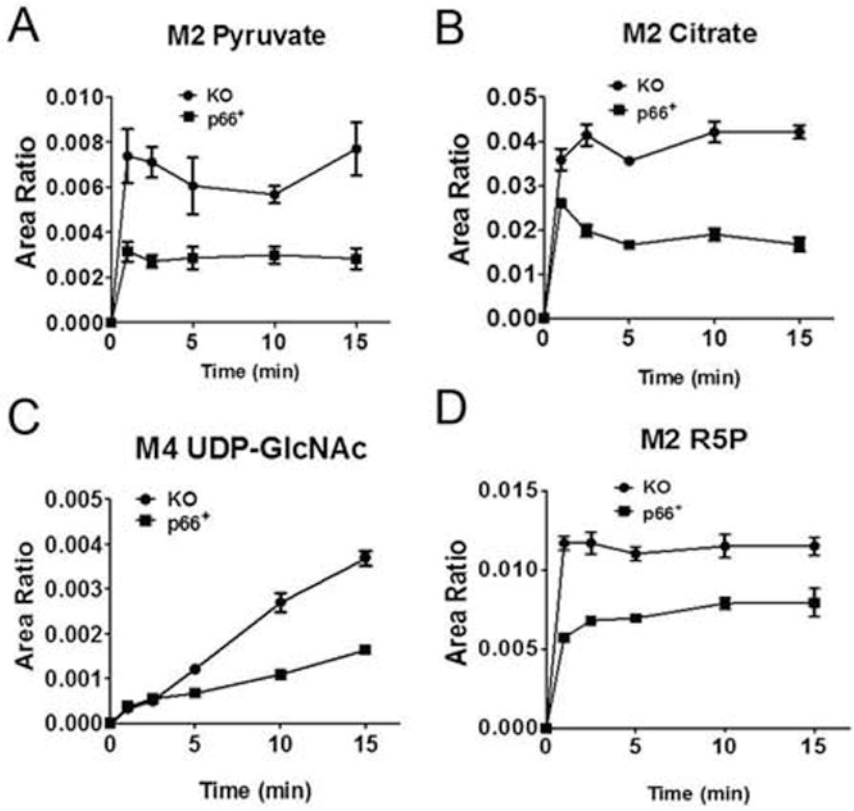

Fig. 5. Glucose flux in p66Shc KO and p66^{+} MEFs

(A-D) Relative amounts of ^{13}C-labeled pyruvate (A), citrate (B), and the pentose phosphate pathway intermediates E4P (C) and R5P (D) after incubating cells with [1,2-$^{13}C_2$] labeled glucose for the indicated time points. Data are represented as the ratio of ^{13}C-labeled metabolites to an internal standard (D7-glucose). Error bars represent SD of at least three independently prepared samples with statistical significance $p < 0.05$.

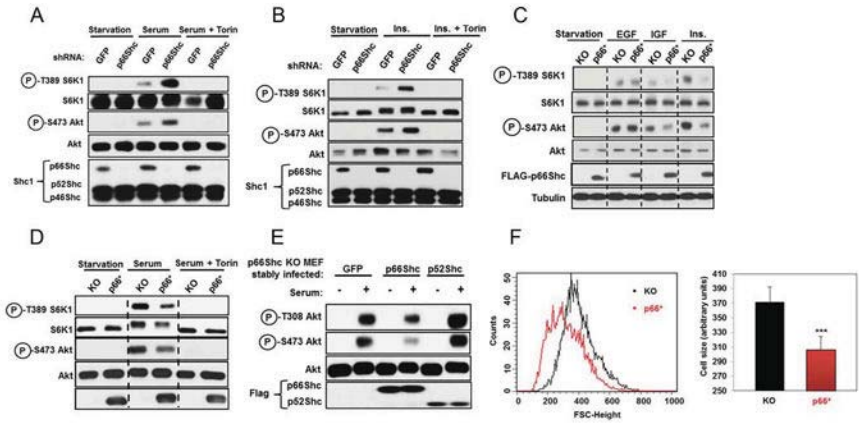

Fig. 6. p66Shc inhibits mTOR activation and cell size

(A) Effect of p66Shc on mTORC1-S6K1 and mTORC2-Akt activation. HeLa cells stably transfected with indicated shRNAs were serum starved, treated with either DMSO or Torin for 1 h, and then stimulated with serum (10 min). Cell lysates were analyzed for the indicated proteins and phosphorylation states by immunoblotting. N = 3 biological replicates. (B) Experiment was done as in (A) but cells were stimulated with 100 nM insulin (10 min). N = 3 biological replicates. (C) Effect of reconstitution of p66Shc expression in p66Shc KO MEFs on mTOR activation in response to EGF, insulin, and IGF1 stimulation. Serum-starved cells were stimulated with 100 nM EGF, IGF, or insulin (10 min). N = 3 biological replicates. (D) Experiment was done as in (C) but cells were stimulated with serum. N = 3 biological replicates. (E) Stable expression of retroviral FLAG-p66Shc, but not FLAG-p52Shc, in p66Shc null cells inhibits the mTOR pathway. Experiment was done as in (C). N = 3 biological replicates. (F) Cell size distribution of KO and $p66^{+}$ MEFs using flow cytometry forward scattering (right). Average cell size of KO and $p66^{+}$ from three independent experiments is represented (left), *** $p < 0.001$.

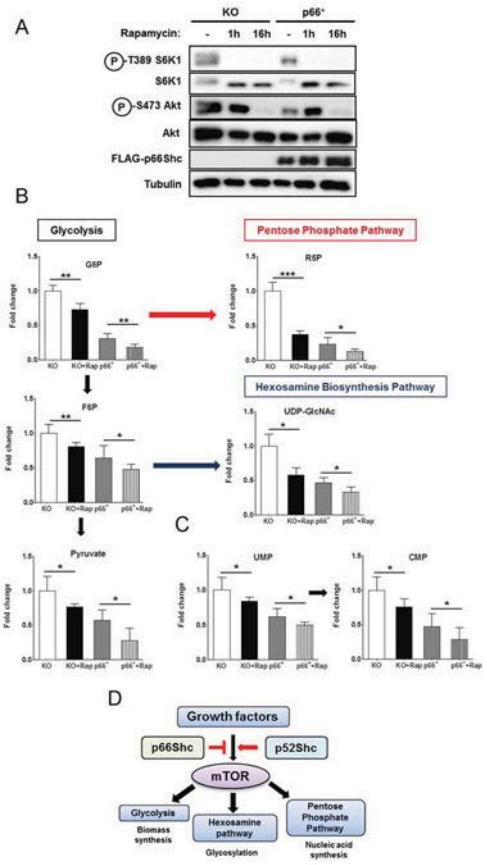

Fig. 7. mTOR mediates the effects of p66Shc on glycolytic and pyrimidine metabolism

(A) Rapamycin treatment for 16 h is sufficient to inhibit both mTORC1 and mTORC2 signaling in p66Shc KO and p66^{+} MEFs. Cell lysates were analyzed for the indicated proteins and phosphorylation states by immunoblotting. N = 3 biological replicates. (B) p66Shc KO and p66^{+} MEFs were treated with vehicle or rapamycin for 16 h, and amounts of glycolysis, hexosamine biosynthesis, and pentose phosphate pathways metabolic intermediates were quantified by LC-MS/MS (ANOVA analysis, N = 3 biological replicates). (C) Fold change of UMP and CMP pyrimidine metabolites. Cells were treated as in (B). (D) Model for role of p66Shc in inhibiting growth factor signaling to glycolytic metabolism and biosynthetic pathways through inhibiting mTOR activation. Error bars represent SD of three independently prepared samples (* $p < 0.05$, ** $p < 0.01$, *** $p < 0.001$).

Table 1

The 10 metabolites that showed the most statistically significant changes of $p66^{+}$ over KO MEFs. N = 3 biological replicates. FDR: False discovery rate.

Metabolite	Fold change	p-value	FDR
Dihydroxyacetone phosphate (DHAP)	0.23	2.44E-05	0.000244
Fructose 6-phosphate (F6P)	0.29	7.64E-05	0.000270333
Glucose 6-phosphate (G6P)	0.36	8.11E-05	0.000270333
Fructose 1,6-bisphosphate (F1,6BP)	0.29	0.000207	0.000452
Malonyl Co-enzyme A (MCoA)	0.30	0.000226	0.000452
Erythrose-4-phosphate (E4P)	0.26	0.000598	0.000915714
$NADH/NAD^{+}$	0.34	0.000641	0.000915714
Acetyl Co-enzyme A (ACoA)	0.29	0.001544	0.00193
2′-Deoxycytidine 5-triphosphate (dCTP)	0.41	0.00265	0.002944444
Uridine 5-triphosphate (UTP)	0.45	0.003853	0.003853